ARL-TR-95-26

Copy No. 11

New Multiple Scatter Model of the Ocean Sediment

Final Report under Grant N00014-94-1-0438
Multiple Scatter Theory of Ocean Sediments

Dennis J. Yelton
Morris Stern
Nicholas P. Chotiros

Applied Research Laboratories
The University of Texas at Austin
P. O. Box 8029 Austin, TX 78713-8029

15 September 1995

Final Report

1 January - 31 August 1995

Approved for public release;
distribution is unlimited.

Prepared for:
Office of Naval Research
Department of the Navy
Arlington, VA 22217-5660

REPORT DOCUMENTATION PAGE

Form Approved
OMB No. 0704-0188

1. AGENCY USE ONLY (Leave blank)	2. REPORT DATE	3. REPORT TYPE AND DATES COVERED
	15 Sep 95	final 1 Jan - 31 Aug 95

4. TITLE AND SUBTITLE
New Multiple Scatter Model of the Ocean Sediment, Final Report under Grant N00014-94-1-0438, Multiple Scatter Theory of Ocean Sediments

5. FUNDING NUMBERS
N00014-94-1-0438

6. AUTHOR(S)
Yelton, Dennis J. Stern, Morris Chotiros, Nicholas P.

7. PERFORMING ORGANIZATION NAMES(S) AND ADDRESS(ES)
Applied Research Laboratories
The University of Texas at Austin
P.O. Box 8029
Austin, Texas 78713-8029

8. PERFORMING ORGANIZATION REPORT NUMBER
ARL-TR-95-26

9. SPONSORING/MONITORING AGENCY NAME(S) AND ADDRESS(ES)
Office of Naval Research
Department of the Navy
Arlington, VA 22217-5660

10. SPONSORING/MONITORING AGENCY REPORT NUMBER

11. SUPPLEMENTARY NOTES

12a. DISTRIBUTION/AVAILABILITY STATEMENT
Approved for public release; distribution is unlimited.

12b. DISTRIBUTION CODE

13. ABSTRACT (Maximum 200 words)
(see reverse side)

14. SUBJECT TERMS
Biot theory
bottom backscatter
layered media
multiscatter
poroelastic media

15. NUMBER OF PAGES
57

16. PRICE CODE

17. SECURITY CLASSIFICATION OF REPORT	18. SECURITY CLASSIFICATION OF THIS PAGE	19. SECURITY CLASSIFICATION OF ABSTRACT	20. LIMITATION OF ABSTRACT
UNCLASSIFIED	UNCLASSIFIED	UNCLASSIFIED	SAR

13.

The reflection and scattering properties of an inhomogeneous poroelastic medium were studied via numerical simulation. The inhomogeneous medium was modeled as an ensemble average of randomly layered poroelastic material. Each layer represented a granular material of a particular grain size. The thickness of each layer was related to the associated grain size and porosity by a conservation of mass relationship. Lateral variations in grain size were approximated by performing a coherent ensemble average of results from several realizations of the randomly stratified medium. Poroelastic medium parameters were chosen to represent water-saturated sand. The mean and standard deviation of the grain size distribution were chosen to match existing experimental data so that the model could be tested. Specifically, the inhomogeneous medium was modeled as bounded by a homogeneous water half-space on the source side, and a homogeneous poroelastic half-space of equivalent average porosity on the other side. Reflected signals were computed for 500 kHz and 1 MHz normally incident plane waves. Coherent and random components of the reflected signal were calculated. The coherent part was directly related to the reflection coefficient. The random component was related to the scattering strength of the medium. It was found to increase with the mean grain size diameter, consistent with previous experimental results.

TABLE OF CONTENTS

This page intentionally left blank.

LIST OF FIGURES

This page intentionally left blank.

PREFACE

This is the final report on work that Applied Research Laboratories, The University of Texas at Austin (ARL:UT), was tasked to perform under Grant N00014-94-1-0438, entitled "Multiple Scatter Theory of Ocean Sediments."

This page intentionally left blank.

1. OBJECTIVE

The goal of this study is to investigate the extent to which sediment granularity can account for the attenuation and scattering that has been observed in ocean sediments, particularly water-saturated sand. Typically, a couple of devices are employed to match theory to experimental measurements of attenuation and scattering; the attenuation is accounted for in terms of a complex bulk modulus, and the scattering is modeled as a random field of point scatterers, in which the scattering strength is adjusted to match the measured data. Both devices have very little physical basis. Our hypothesis is that both attenuation and scattering might be explained in terms of acoustic interaction with the sediment grains. The viscoelastic theory of acoustic propagation in a solid is not a suitable starting point since it does not possess a mechanism that can account for the interaction between pore fluid and solid particles. Our starting point is Biot's theory of acoustic propagation in a poroelastic medium. It contains the basic mechanisms of acoustic interaction between the solid matrix and pore liquid as far as forward propagation is concerned, but it does not have any mechanism to account for scattering and any associated losses due to granularity. Our intention is to extend Biot's theory to include the effects of granularity. In this initial study, we will use a brute force, numerical simulation approach to obtain results quickly. The results of this initial study were compared with experimental data to test the feasibility of our hypothesis. The comparison, as it turned out, was very encouraging, and provides a solid foundation for proceeding to the next phase of the investigation, which will be directed towards obtaining analytical relationships.

This page intentionally left blank.

2. INTRODUCTION

Current models of acoustic bottom backscatter from sandy sediments are based on composite roughness and volume scattering effects from sediments modeled as fluids.[1-3] However, recent bottom penetration experiments by Chotiros[4-6] have shown that Biot's theory,[7,8] based on the propagation of sound through a fluid-filled porous solid matrix, better explains the conduction of acoustic energy into the sediment. This conduction process is an important factor in any model of scattering by sediment volume, making it plausible to apply Biot's theory to sediment scattering. Biot's theory predicts acoustic propagation through a poroelastic medium as a coupled wave motion within the solid and the pore fluid. The medium is modeled as a solid with tubular pores, as illustrated in Fig. 2.1. The propagating wave, in the direction of the pore tubes, can be decomposed into three components -- a fast and a slow compression wave, and a shear wave. The equations of motion, in a form used by Stern, Bedford, and Millwater[9] (correcting for typographical errors), are

$$\mu\nabla^2\mathbf{u} + (H-\mu)\nabla(\nabla\cdot\mathbf{u}) - C\,\nabla(\nabla\cdot\mathbf{w}) = \rho\ddot{\mathbf{u}} - \rho_f\ddot{\mathbf{w}} \quad , \qquad (2.1)$$

$$C\nabla(\nabla\cdot\mathbf{u}) - M\nabla(\nabla\cdot\mathbf{w}) = \rho_f\ddot{\mathbf{u}} - \frac{c\rho_f}{\beta}\ddot{\mathbf{w}} - \frac{F^*\eta}{\kappa}\dot{\mathbf{w}} \quad , \qquad (2.2)$$

where **u** is the displacement vector of the solid frame, **w** is the negative porosity times the displacement vector of the pore fluid relative to the solid frame, β is the porosity of the solid frame, ρ_f is the mass density of the pore fluid, ρ is the mass density of the saturated sediment, μ is the shear modulus of the solid frame, c is the virtual mass coefficient of fluid motion, η is the viscosity of the fluid, and κ is the permeability of the solid frame. C, H, and M are constitutive coefficients depending on β, μ, and the bulk moduli of the pore fluid, grain material, and the saturated sediment. F is a frequency-dependent dynamic correction term describing the frictional force due to the relative motion of the solid and fluid, as given by Biot.[7,8] The relationships between the parameters of Eqs. (2.1) and (2.2) are given in Appendix A. In order to match the calculated acoustic wave attenuations to measured values, imaginary terms must be added to the frame bulk and shear moduli. Furthermore, the theory has no mechanism for scattering because the pores are modeled as parallel smooth walled tubes that are perfectly aligned with the direction of wave propagation.

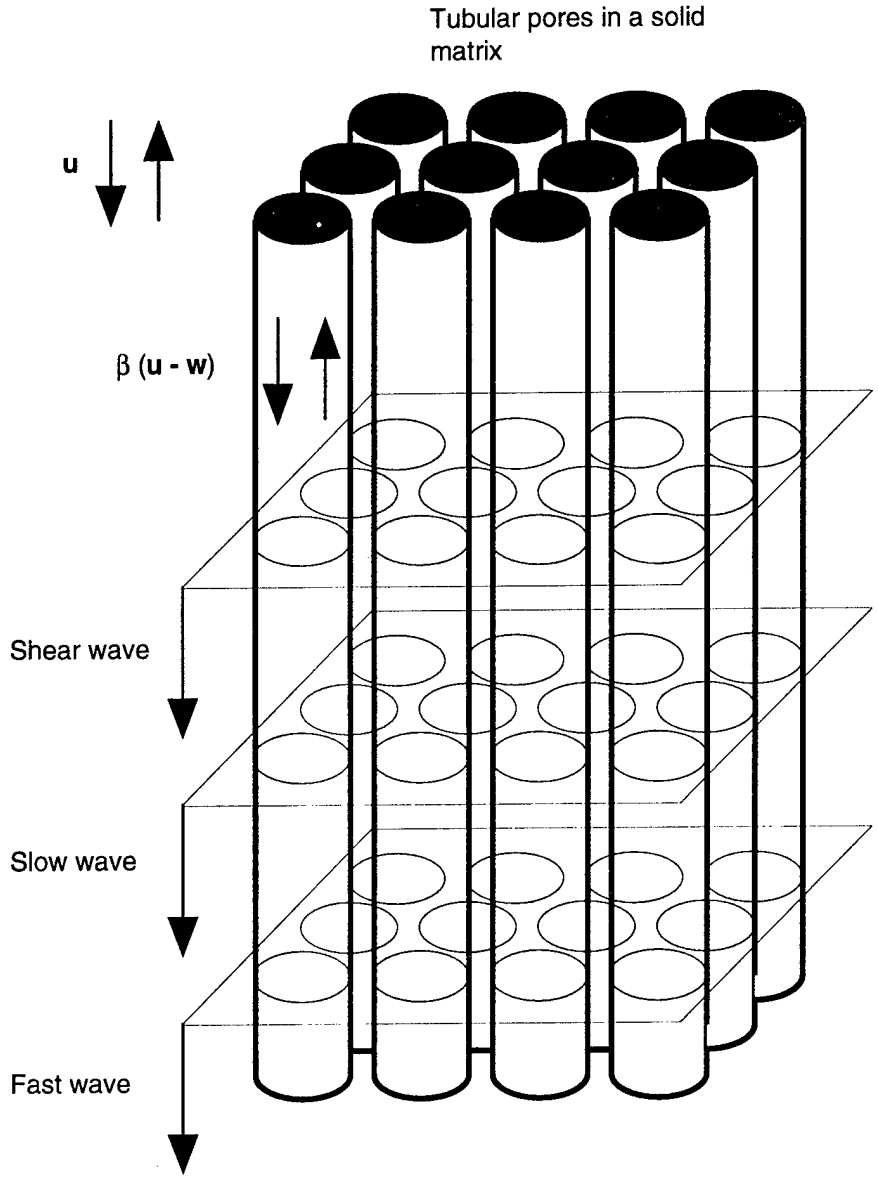

Figure 2.1
Illustration of Biot's theory of acoustic propagation through a poroelastic medium.

When **u** and **w** are written in terms of vector and scalar potentials, the above two equations separate into four coupled vector partial differential equations. For homogeneous media, the vector and scalar potentials have plane wave solutions. At a fluid/poroelastic interface, there are four boundary conditions imposed on these solutions -- continuity of fluid pressure, continuity of shear traction, continuity of normal traction, and continuity of normal fluid displacement. At a poroelastic/poroelastic interface there are two additional boundary conditions -- continuity of tangential solid displacement and continuity of normal solid displacement. The mathematical formulation of the differential equations and boundary conditions governing the vector and scalar potentials are clearly illustrated by Stern, Bedford, and Millwater,[9] and are outlined in Appendix A.

This page intentionally left blank.

3. MODEL

We now present a multiple scatter model of the ocean sediment. In this model, the ocean sediment is represented as a finite granular medium bounded above by a homogeneous fluid half-space (water) and below by a homogeneous poroelastic half-space. The poroelastic half-space has properties given in Table 3.1, which were recently determined by Chotiros[4] for sound propagating through water-saturated sand. Likewise, the fluid half-space has properties denoted by the fluid properties in Table 3.1. Before continuing, the terms "granular" and "poroelastic" need some clarification. In the context of this study, the term "poroelastic" refers to a medium that follows Biot's theory of acoustic propagation as described by Eqs. (3.1) and (3.2), in which the pores are modeled as parallel tubes as described in Fig. 2.1. The term "granular" refers to a poroelastic medium that is consistent with Biot's theory, and which, in addition, the pore diameter may vary, thus giving rise to scattering mechanisms associated with the granularity.

A randomly packed granular medium, such as the ocean sediment, is essentially a three-dimensional medium that will reflect, transmit and, most importantly, scatter an incident acoustic wave. Ideally, a fully three-dimensional mathematical model is required, but it would be very expensive to develop and compute. However, it is noted that the inhomogeneities in ocean sediments, particularly sand beds, are structured as horizontal lenses, as illustrated in Fig. 3.1(a). We have chosen to model the lenses as an ensemble of random, horizontally layered, poroelastic media, as illustrated in Fig. 3.1(b), whose acoustical response, when summed, will approximate that of a fully three-dimensional model. This model ignores the edge effects at the periphery of the lenses, which are expected to be small. The approach is attractive because a horizontally layered medium, being essentially a one-dimensional problem, is quite simple to compute, as shown in Appendix B. Even an ensemble of several random realizations is still quite economical computationally.

Each realization of a randomly layered poroelastic medium consists of a series of poroelastic layers of differing properties, sandwiched between an upper fluid half-space and a lower uniform poroelastic half-space, as illustrated in Fig. 3.2. Within the randomly layered medium, the i^{th} layer corresponds to

Table 3.1
Material properties of the homogeneous Biot half-space.

Fluid viscosity (η)	1.00×10^{-3} kg/m-s
Fluid mass density (ρ_f)	1000 kg/m^3
Fluid bulk modulus (K_f)	2.25×10^9 Pa
Grain mass density (ρ_g)	2650 kg/m^3
Grain bulk modulus (K_r)	7.00×10^9 Pa
Frame shear modulus (μ_0)	2.61×10^7 Pa
Frame bulk modulus (K_{b0})	5.30×10^9 Pa
Frame porosity (β)	0.36
Frame shear log decrement (δ_s)	0.15
Frame bulk log decrement (δ)	0.15

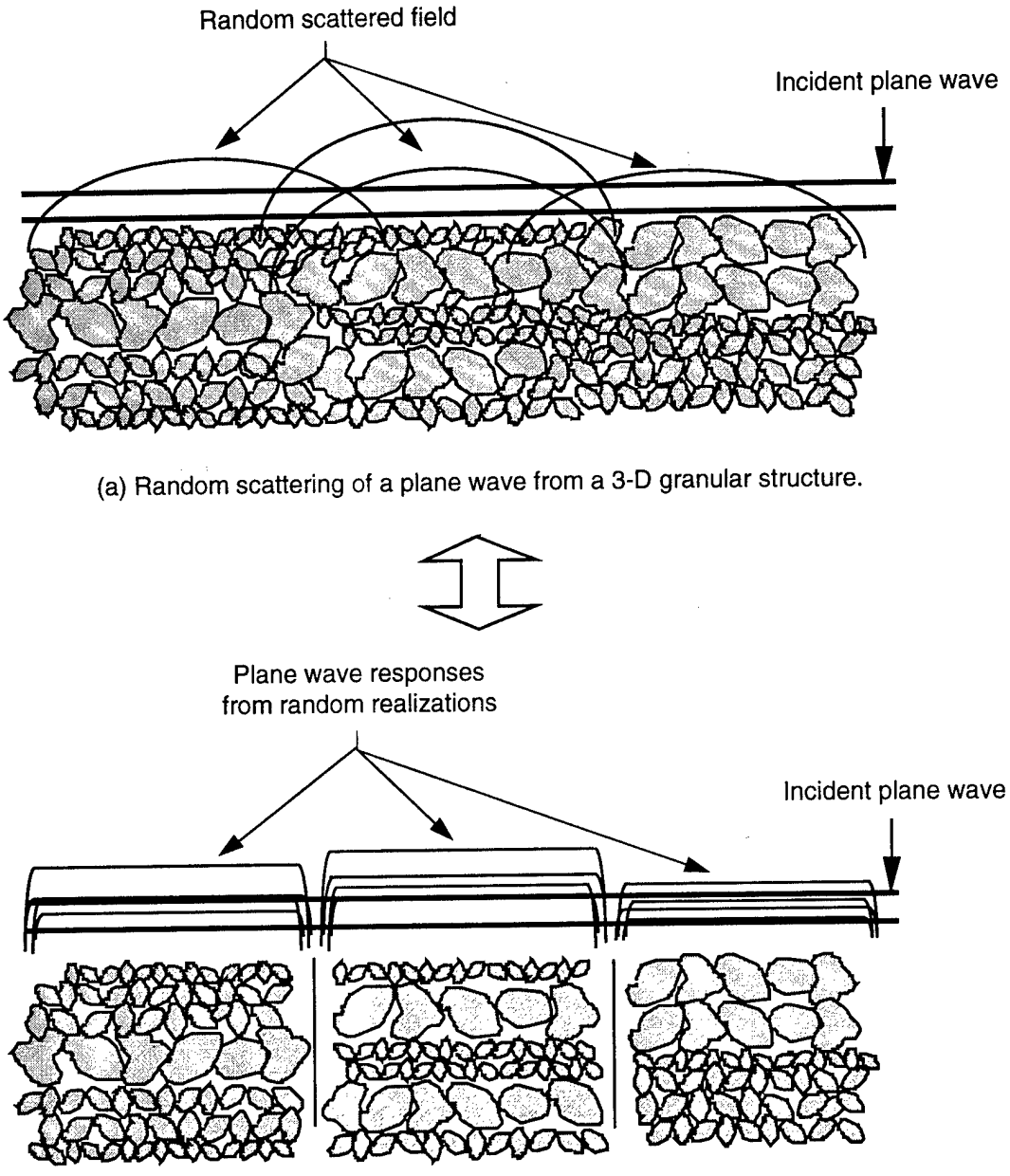

(a) Random scattering of a plane wave from a 3-D granular structure.

(b) Summation of scattered signals from ensemble of 1-D structures.

Figure 3.1
Simulation of plane wave scattering from a 3-D granular structure with an ensemble of 1-D structures.

ARL - UT
AS-95-1101
DJY/RFO
12-95/svr

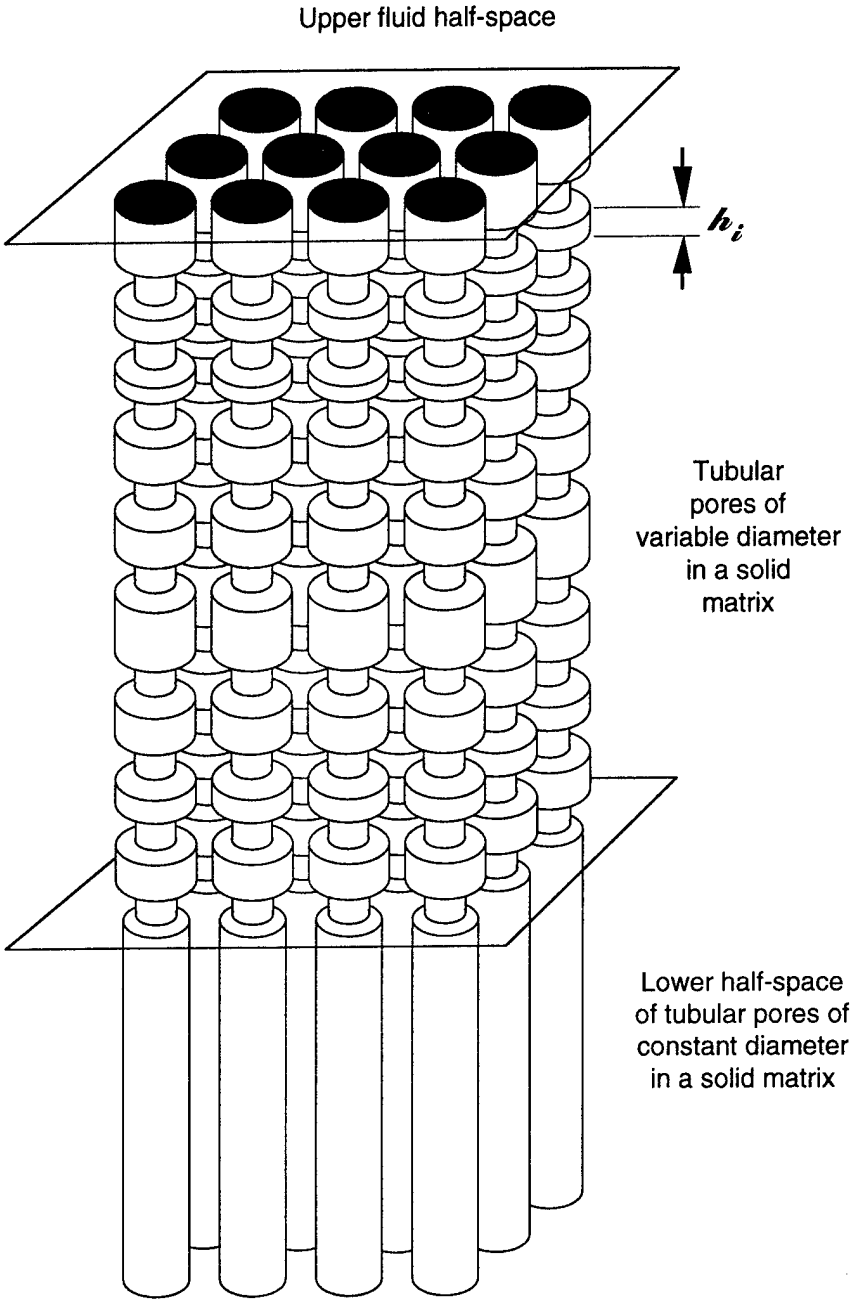

Figure 3.2
A randomly layered Biot medium, bounded above by a homogeneous fluid half-space and below by a homogeneous Biot half-space.

a mono-layer of granular material of uniform, but randomly chosen, grain diameter, a_i. For a given grain size, greater layer thickness implies greater fluid volume within the layer, and hence greater porosity for the layer. Therefore, a certain correlation between the thickness h_i and porosity β_i of the i^{th} layer within the granular medium is postulated. The layer porosity is simply the ratio of the fluid volume to the total volume of the layer.

$$\beta_i = \frac{h_i - a_i}{h_i} = 1 - \frac{a_i}{h_i} \quad . \tag{3.1}$$

The average layer thickness is chosen so that average porosity of the granular medium is the same as that of the homogeneous poroelastic half-space, as given in Table 3.1.

The properties that are dependent on porosity and grain diameter are computed according to the method described by Chotiros.[5] Other material properties of each layer within the granular medium match those of the homogeneous Biot half-space. Further details are given in Appendix A. Of particular significance, within the randomly layered poroelastic medium, the log decrements are set to zero (i.e., the imaginary parts of the bulk and shear moduli are set to zero), in the expectation that the acoustic interactions with the pore size variations will provide the necessary loss and scattering mechanism that will properly account for the experimentally observed attenuation and scattering phenomena.

This page intentionally left blank.

4. SIMULATION PROCEDURE

The purpose of this simulation was to verify the feasibility of the model described above by comparing the model predictions of reflection loss and scattering strength with experimental data. The simulation parameters were chosen to allow comparison of the results with the experimental work of Nolle[10] and Mifsud,[11] who made measurements at 500 kHz and 1 MHz. The mean and standard deviations of the grain sizes of the sand samples used in their experiments are shown in Table 4.1. For simplicity, only the case of normal incidence was considered.

It was assumed that the grain size distribution is a log-normal function. Hence, the distribution is completely specified by two free parameters, its mean and standard deviations. For simulation purposes, a number of mean grain sizes between 120 μm and 640 μm were chosen. The dimensionless standard deviation was then determined by linear interpolation of the corresponding experimental values in Table 4.1.

Table 4.1
The mean and dimensionless standard deviations for the grain size distributions of the granular medium. (The dimensionless standard deviations for intermediate grain diameters are determined by linear interpolation.)

Mean diameter (μm)	Dimensionless standard deviation
120	0.28
170	0.17
400	0.15
640	0.11

In the absence of any further information, the dimensionless layer thickness was arbitrarily chosen to have the same statistical distribution as the grain size, but the grain size and layer thickness were treated as independent variables. The mean of the thickness distribution was chosen so that the mean porosity of a many-layered sediment, as determined from Eq. (4.1), was the same as that of the homogeneous poroelastic half-space, i.e., 0.36. Thus,

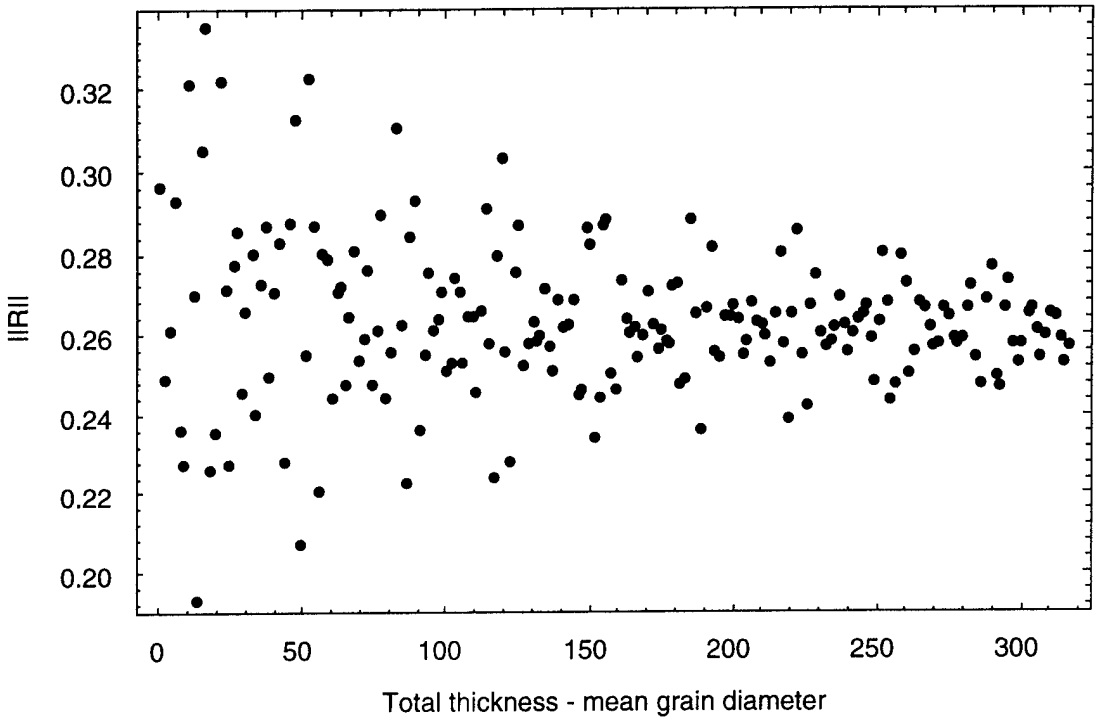

Figure 4.1
An example showing the variation of the reflection amplitude with the total sediment thickness (mean grain diameter = 120 μm).

$$\left\langle \frac{a}{h} \right\rangle = 1 - 0.36 = 0.64 \quad . \tag{4.1}$$

Given the grain size and layer thickness distributions, the layered Biot medium was generated layer by layer. The grain size and thickness of each layer were independently chosen at random, consistent with the given distribution functions. The reflection loss was computed as a function of the number of layers, using the procedure given in Appendix A. One realization of such a plot is shown in Fig. 4.1. When the number of layers was small, the reflection amplitude varied wildly with the addition of each new layer. As the number of layers increased, the amplitude of the reflected signal appeared to converge about a mean value.

To account for lateral variations in a realistic sandy sediment, the reflected signal was computed from an ensemble of random realizations of the same grain size and layer thickness distributions. The ensemble average of the reflected signal was used to compute the reflection coefficient. It was implicitly assumed that there is no correlation between the lateral depth profile variations. Typically, 25 random realizations were generated for each grain size distribution. The reflection coefficient was calculated from the mean value of the complex reflected signal, i.e., its coherent component, as given by $||\langle R \rangle||^2$. The scattering strength was calculated from the variation in reflected amplitudes, i.e., the random component, as given by

$$S = 10 \log\left(\left\langle \|R - \langle R \rangle\|^2 \right\rangle\right) = 10 \log\left(\left\langle \|R\|^2 \right\rangle - \|\langle R \rangle\|^2\right) \quad . \tag{4.2}$$

Due to the one-dimensional nature of these simulations, the scattered energy was all directed back to the source of the incident wave. But, experimentally, the measured scattering at a water-sediment interface is a three-dimensional process in which energy is scattered within a hemispherical sector of 2π steradians. To compensate for this inherent discrepancy, the simulated scattering strength was offset by a precalculated amount that depends on the incident frequency. The details of this calculation are given in Appendix C.

This page intentionally left blank.

5. RESULTS

5.1 REFLECTION LOSS

As illustrated in Fig. 4.1, the norm of the reflection amplitude varied about a mean value as the number of layers in the sediment increased. The values were averaged over 575 realizations of the granular sediment. The result was estimated to be 0.268, equivalent to -11.4 dB, which is in good agreement with the measured value by Nolle[10] and Mifsud[11] of -11 dB. No significant deviations from this value were observed between the frequencies or grain sizes used in this study.

5.2 SCATTERING STRENGTH

For incident wave frequencies of both 500 kHz and 1 MHz, scattering strengths were calculated for mean grain diameters ranging from 120 μm to 640 μm. The results are shown superimposed on the experimental data of Nolle in Figs. 5.1 and 5.2.

At 500 kHz, the calculated scattering strength at normal incidence as a function of grain size was in good agreement with the experimental data for mean grain diameters up to about 530 μm. Beyond this, the calculated scattering strength dropped sharply below the experimental values. At the point of divergence, the wavelength of the Biot fast wave was 6.4 mean grain diameters, or about four mean layer thicknesses. This indicates that our model is only valid for grain sizes significantly less than the acoustic wavelength within the sediment.

At 1 MHz, the calculated scattering strength was only in agreement with the experimental data for mean grain diameters up to about 210 μm. At this point of divergence, the wavelength of the Biot fast wave was 8.0 mean grain diameters, or about five mean layer thicknesses. Although these results are consistent with the previous interpretation that the model is valid for grain sizes significantly less than the acoustic wavelength, the range of experimental data points below 210 μm was too small to establish a legitimate trend.

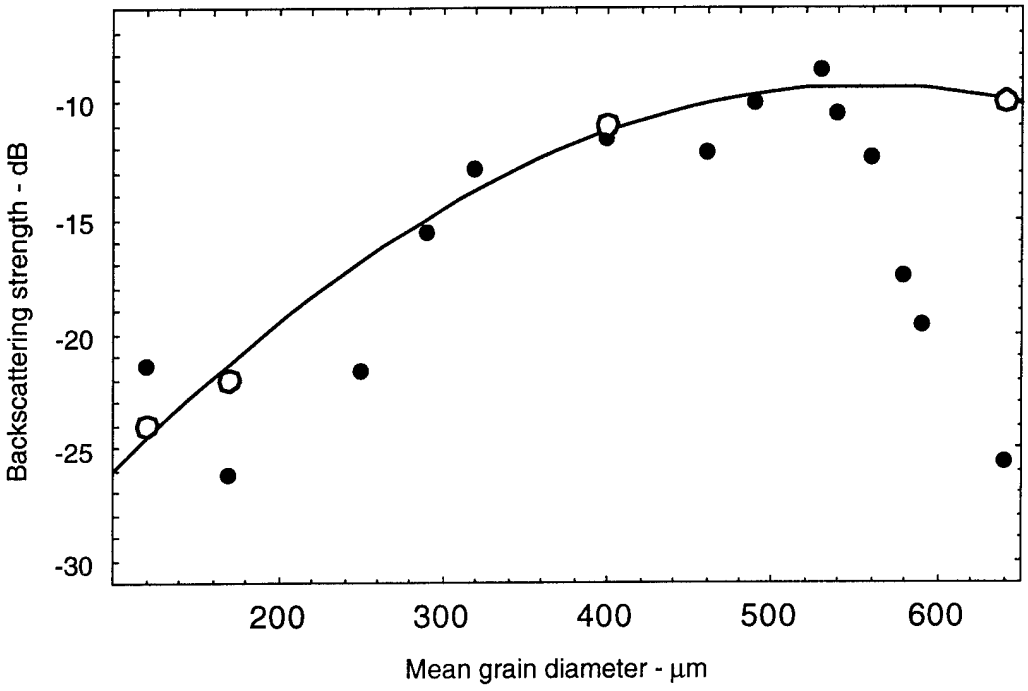

Figure 5.1
Calculated backscattering strength as a function of mean grain diameter at 500 kHz compared with Nolle's experimental data.

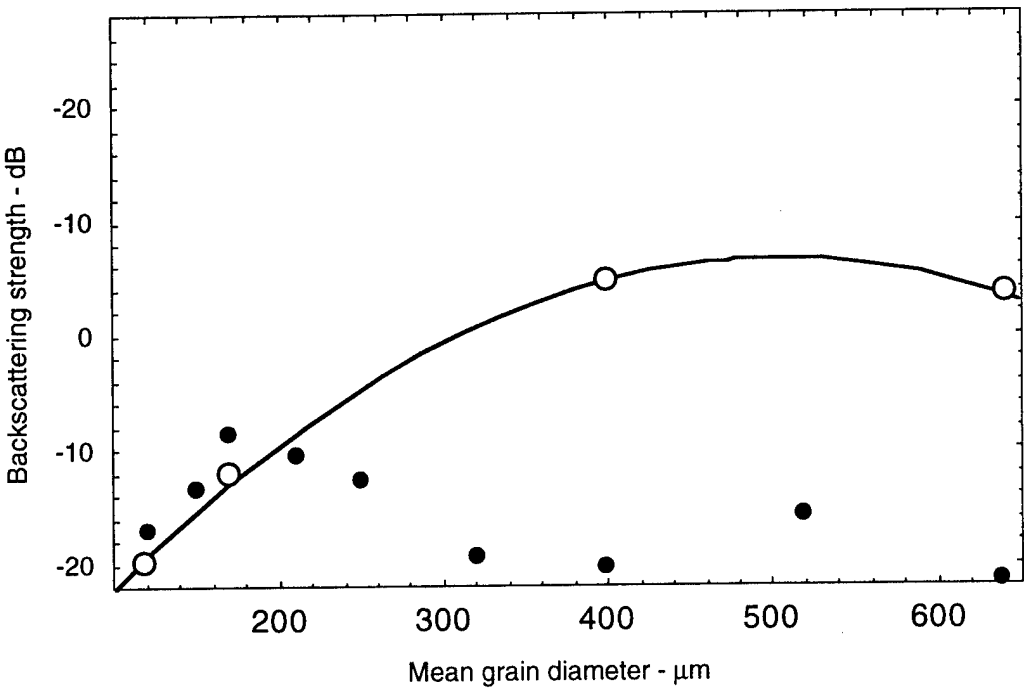

Figure 5.2
Calculated backscattering strength as a function of mean grain diameter at 1 MHz compared with Nolle's experimental data.

This page intentionally left blank.

6. CONCLUSIONS

The effects of granularity have been added to a Biot model of ocean sediments in a numerical simulation by introducing homogeneous layers of random thicknesses on the order of a grain diameter, in which the mean porosity is preserved. Within each layer, conservation of grain volume dictates a linear relationship between the layer thickness, porosity, and grain diameter.

Lateral variations in sediment structure were simulated by coherently averaging the results for several random realizations of a layered poroelastic medium with given grain size and layer thickness distributions. The reflection loss predicted by this model was computed from the coherent component of the ensemble average of the reflected signal, and it was found to be in good agreement with measured values by Nolle. The scattering strength was computed from the random component of the reflected signal, and its values were found to be in agreement with experimental data for mean grain sizes significantly less than the acoustic wavelength within the sediment. However, the simulated scattering strength dropped sharply below the observed values for grain sizes near or greater than the acoustic wavelength. This indicates that the model is only valid for incident waves that yield acoustic wavelengths near or greater than ten times the mean grain diameter of the sediment.

The approach that we have taken is based on sound physical principles. It is a significant extension of Biot's theory of acoustic propagation in porous media, and gives an insight to the processes that give rise to reflection and scattering from a granular medium such as water saturated sand, that is directly applicable to ocean sediments. The above agreement between model predictions and experimental measurement indicates that the approach is feasible. Follow-on work will include computation of wave attenuation due to granularity, which would involve calculation of transmission coefficients through the granular material. Then, we will attempt to derive an analytical model, based on our understanding of the numerical simulation results.

This page intentionally left blank.

ACKNOWLEDGMENTS

A large portion of the computer code used for the simulations was written and tested by Theodore J. Kim, at Applied Research Laboratories, The University of Texas at Austin. This work is supported by the Office of Naval Research, Code 321OA.

This page intentionally left blank.

APPENDIX A
PROBLEM SETUP AND SOLUTION

This page intentionally left blank.

Most of the equations used are the same as those given by Stern, Bedford, and Millwater.[9] There are a few typographical errors in the equations from this reference, which have been corrected. The corrected equations in this appendix are Eqs. (A.5), (A.6), (A.29), (A.45), and (A.46).

The ocean sediment is represented as a finite granular medium bounded above by a homogeneous fluid half-space (water) and below by a homogeneous Biot half-space. The granular medium is composed of homogeneous Biot layers of differing properties and thicknesses, as depicted in Fig. 3.2.

The layers of the finite granular medium are numbered 1 to N, from top to bottom. The homogeneous Biot half-space is layer number $N + 1$, and the fluid medium is number 0. All $N + 1$ Biot layers have identical values for the fluid viscosity (η), fluid mass density (ρ_f), fluid bulk modulus (K_f), grain mass density (ρ_g), grain bulk modulus (K_r), frame shear modulus (μ_0), and frame bulk modulus (K_{b0}). The fluid medium has the same fluid mass density (ρ_f) and fluid bulk modulus (K_f) as the Biot media. These values are given in Table 3.1.

The i^{th} layer of the granular medium corresponds to a mono-layer of granular material of uniform, but randomly chosen, grain size, a_i. The choice of a grain size distribution is the sole free parameter for generating a granular sediment of given total thickness.

In this model there is a correlation between the thickness h_i and porosity β_i of the i^{th} layer within the granular medium. Each layer represents a mono-layer of granular material of uniform grain size. So, for a given grain size, greater layer thickness implies greater fluid volume within the layer, and hence greater porosity for the layer. For a given grain size distribution, the dimensionless layer thickness distribution is identical to that of the grain size distribution. The mean of the layer thickness distribution is chosen so that average porosity of a many-layered granular medium would be the same as for the homogeneous Biot half-space, β_{n+1}. The porosity of the i^{th} layer is simply the ratio of the fluid volume to the total volume of the layer. Due to the effectively one-dimensional character of the simulations in this present study,

we choose

$$\beta_i = 1 - \frac{a_i}{h_i}, \qquad i = 1, 2, ..., N , \tag{A.1}$$

$$\beta_{N+1} = 0.36. \tag{A.2}$$

The skeletal frame's bulk and shear logarithmic decrements are set equal to zero for the first N layers, and set equal to 0.15 for the final semi-infinite layer.

$$\delta_i = \delta_{si} = 0, \qquad i = 1, 2, ..., N , \tag{A.3}$$

$$\delta_{N+1} = \delta_{sN+1} = 0.15 , \tag{A.4}$$

$$K_{bi} = K_{b0}\left(1 - i\frac{\delta_i}{\pi}\right) , \tag{A.5}$$

$$\mu_i = \mu_0\left(1 - i\frac{\delta_{si}}{\pi}\right) . \tag{A.6}$$

The mass density of the saturated sediment is simply

$$\rho_i = (1 - \beta_i)\rho_g + \beta_i \rho_f . \tag{A.7}$$

The constitutive coefficients given in Eqs. (2.1) and (2.2) are

$$M_i = \frac{K_r}{1 - \frac{K_{bi}}{K_r} + \beta_i\left(\frac{K_r}{K_f} - 1\right)} , \tag{A.8}$$

$$C_i = \left(1 - \frac{K_{bi}}{K_r}\right)M_i , \tag{A.9}$$

$$H_i = \left(1 - \frac{K_{bi}}{K_r}\right)C_i + K_{bi} + \frac{4}{3}\mu_i . \tag{A.10}$$

A plane wave of angular frequency ω is incident upon this sediment configuration from above with grazing angle θ. The component of the wave number parallel to the fluid/sediment interface is

$$k = \omega\sqrt{\frac{\rho_f}{K_f}}\cos(\theta) \quad , \tag{A.11}$$

where ρ_f and K_f are the fluid mass density and fluid bulk modulus, as given in Table 2.1. The simulations of the present study concern the effectively one-dimensional case of normal incidence, with $k = 0$.

For the i^{th} layer, the virtual mass coefficient, c, and the permeability, κ, of Eq. (2.2) are given by

$$c_i = 1 + 0.5\frac{1-\beta_i}{\beta_i} \quad , \tag{A.12}$$

and

$$\kappa_i = \frac{\beta_i p_i^2}{20} \quad , \tag{A.13}$$

where p_i is the pore size parameter, given by

$$p_i = \frac{\beta_i a_i}{3(1-\beta_i)}, \quad i = 1, 2, 3, \ldots, N \quad , \tag{A.14}$$

$$p_{N+1} = \frac{\beta_{N+1}\langle a\rangle}{3(1-\beta_{N+1})} \quad , \tag{A.15}$$

and $\langle a\rangle$ is the mean of the grain size distribution.

The dynamic correction term F, of Eq. (2.2) depends on the incident frequency. For the i^{th} layer, it can be written as

$$F_i = \frac{\xi_i T(\xi_i)}{4\left[1 - \frac{2T(\xi_i)}{i\xi_i}\right]} \quad , \tag{A.16}$$

where

$$T(\xi_i) = \frac{\mathrm{ber}'(\xi_i) + i\,\mathrm{bei}'(\xi_i)}{\mathrm{ber}(\xi_i) + i\,\mathrm{bei}(\xi_i)} \quad , \tag{A.17}$$

and

$$\xi_i = p_i \sqrt{\frac{\omega \rho_f}{\eta}} \quad . \tag{A.18}$$

The horizontal position coordinate is denoted by x. The vertical position coordinate increases downward, and for the i^{th} layer is denoted by z_i. At the upper boundary of the i^{th} Biot layer, $z_i = 0$. The first vertical coordinate z_0 within the fluid medium is set equal to zero at the fluid/sediment interface.

The solid displacement term **u** and the relative solid/fluid displacement term **w**, from Eqs. (2.1) and (2.2), can be expressed in terms of scalar and vector potentials:

$$\mathbf{u} = \nabla \Phi_s + \nabla \times \Psi_s \quad , \tag{A.19}$$

$$\mathbf{w} = \nabla \Phi_f + \nabla \times \Psi_f \quad . \tag{A.20}$$

The scalar and vector potentials for the i^{th} layer can be written as

$$\Phi_{si} = \phi_{si}(z_i)\, e^{i(kx - \omega t)} \quad , \tag{A.21}$$

$$\Phi_{fi} = \phi_{fi}(z_i)\, e^{i(kx - \omega t)} \quad , \tag{A.22}$$

$$\Psi_{si} = \psi_{si}(z_i)\, e^{i(kx - \omega t)}\, \mathbf{j} \quad , \tag{A.23}$$

$$\Psi_{fi} = \psi_{fi}(z_i)\, e^{i(kx - \omega t)}\, \mathbf{j} \quad . \tag{A.24}$$

Inserting these into Biot's equations of motion, Eqs. (2.1) and (2.2), yields a set of four coupled equations for ϕ and ψ:

$$\ddot{\phi}_{si} + v_{si}^2 \phi_{si} - \zeta_{si}^2 \phi_{fi} = 0 \quad , \tag{A.25}$$

$$\ddot{\phi}_{fi} + \chi_{fi}^2 \phi_{fi} - \lambda_{fi}^2 \phi_{si} = 0 \quad , \tag{A.26}$$

$$\ddot{\psi}_{si} + l_{si}^2 \psi_{si} = 0 \quad , \tag{A.27}$$

$$\psi_{fi} = \gamma_i \psi_{si} \quad , \tag{A.28}$$

where

$$\alpha_i = i \frac{F_i^* \eta \omega}{\kappa_i} \quad , \tag{A.29}$$

$$\overline{\rho}_i = \frac{c_i \rho_f}{\beta_i} \quad , \tag{A.30}$$

$$\gamma_i = \frac{\rho_f \omega^2}{\overline{\rho}_i \omega^2 + \alpha_i} \quad , \tag{A.31}$$

$$d_i = M_i H_i - C_i^2 \quad , \tag{A.32}$$

$$\kappa_{si}^2 = \frac{\left(M_i \rho_i - C_i \rho_f\right)}{d_i} \omega^2 \quad , \tag{A.33}$$

$$\kappa_{fi}^2 = \frac{\left(H_i \overline{\rho}_i - C_i \rho_f\right)}{d_i} \omega^2 \quad , \tag{A.34}$$

$$\beta_{si}^2 = \frac{\left(\rho_i - \gamma_i \rho_f\right)}{\mu_i} \omega^2 \quad , \tag{A.35}$$

$$\lambda_{si}^2 = \frac{\left(M_i \rho_f - C_i \overline{\rho}_i\right)}{d_i} \omega^2 \quad , \tag{A.36}$$

$$\lambda_{fi}^2 = \frac{\left(H_i \rho_f - C_i \rho_i\right)}{d_i} \omega^2 \quad , \tag{A.37}$$

$$\chi_{fi}^2 = \kappa_{fi}^2 - k^2 + \frac{H_i \alpha_i}{d_i} \quad , \tag{A.38}$$

$$\zeta_{si}^2 = \lambda_{si}^2 - \frac{C_i \alpha_i}{d_i} \quad , \tag{A.39}$$

$$\nu_{si}^2 = \kappa_{si}^2 - k^2 \quad , \tag{A.40}$$

$$l_{si}^2 = \beta_{si}^2 - k^2 \quad . \tag{A.41}$$

The solutions to Eqs. (A.25) - (A.27) are plane waves of the form

$$\phi_{si}(z_i) = A_{+si} e^{i l_{1i} z_i} + B_{+si} e^{i l_{2i} z_i} + A_{-si} e^{-i l_{1i} z_i} + B_{-si} e^{-i l_{2i} z_i} \quad , \tag{A.42}$$

$$\phi_{fi}(z_i) = \delta_{1i} A_{+si} e^{i l_{1i} z_i} + \delta_{2i} B_{+si} e^{i l_{2i} z_i} + \delta_{1i} A_{-si} e^{-i l_{1i} z_i} + \delta_{2i} B_{-si} e^{-i l_{2i} z_i} \quad , \tag{A.43}$$

$$\psi_{si}(z_i) = C_{+si} e^{i l_{si} z_i} + C_{-si} e^{-i l_{si} z_i} \quad , \tag{A.44}$$

where

$$l_{1i}^2 = \frac{1}{2}\left(\chi_{fi}^2 + \nu_{si}^2\right) - \sqrt{\frac{1}{4}\left(\chi_{fi}^2 - \nu_{si}^2\right)^2 + \lambda_{fi}^2 \zeta_{si}^2} \quad , \tag{A.45}$$

$$l_{2i}^2 = \frac{1}{2}\left(\chi_{fi}^2 + \nu_{si}^2\right) + \sqrt{\frac{1}{4}\left(\chi_{fi}^2 - \nu_{si}^2\right)^2 + \lambda_{fi}^2 \zeta_{si}^2} \quad , \tag{A.46}$$

$$\delta_{1i} = \frac{\nu_{si}^2 - l_{1i}^2}{\zeta_{si}^2} \quad , \tag{A.47}$$

$$\delta_{2i} = \frac{\nu_{si}^2 - l_{2i}^2}{\zeta_{si}^2} \quad . \tag{A.48}$$

The terms l_{1i}, l_{2i}, and l_{si} are the wave numbers of the Biot fast, slow, and shear waves within the i^{th} layer, respectively. The "+" and "-" coefficients are the amplitudes of the downward-moving (transmitted) waves and the upward-moving (reflected) waves within the i^{th} layer, respectively.

Let R be the reflection amplitude of the wave within the fluid medium. The unknowns of the problem are R, and the As, Bs, and Cs of Eqs. (A.42) - (A.44). Since there are no reflections within the homogeneous semi-infinite Biot medium, we have

$$A_{-sN+1} = B_{-sN+1} = C_{-sN+1} = 0. \quad . \tag{A.49}$$

Thus, there are a total of $6N + 4$ unknowns, which satisfy the $6N + 4$ linear algebraic equations generated by the boundary conditions.

The boundary conditions pertain to continuity of fluid pressure, traction, fluid displacement, and solid displacement. Within the Biot media, the fluid (pore) pressure is

$$p_i = \left[M_i\left(\phi_{fi}'' - k^2\phi_{fi}\right) - C_i\left(\phi_{si}'' - k^2\phi_{si}\right)\right] e^{i(kx - \omega t)},\ i = 1, 2, \ldots, N+1 \quad , \tag{A.50}$$

and within the fluid medium it is

$$p_0 = \rho_f \omega^2 (1 + R)\, e^{i(kx - \omega t)} \quad . \tag{A.51}$$

The shear traction within the Biot media is given by

$$(\sigma_i)_{xz} = \mu_i\left[2ik\phi_{si}' - \left(\psi_{si}'' + k^2\psi_{si}\right)\right] e^{i(kx - \omega t)},\ i = 1, 2, \ldots, N+1 \quad , \tag{A.52}$$

and within the fluid medium it is

$$(\sigma_0)_{xz} = 0 \quad . \tag{A.53}$$

The normal traction is

$$(\sigma_i)_{zz} = [H_i(\phi_{si}'' - k^2\phi_{si}) + 2ik\mu_i(\psi_{si}' - ik\phi_{si}) - C_i(\phi_{fi}'' - k^2\phi_{fi})]\, e^{i(kx - \omega t)}, \quad i = 1, 2, ..., N+1, \quad , \tag{A.54}$$

$$(\sigma_0)_{zz} = -p_0 = -\rho_f \omega^2 (1 + R)\, e^{i(kx - \omega t)} \quad , \tag{A.55}$$

and the normal fluid displacement is given by

$$(u_i)_z - (w_i)_z = [(\phi_{si}' + ik\psi_{si}) - (\phi_{fi}' + ik\psi_{fi})]\, e^{i(kx - \omega t)}, \quad i = 1, 2, ..., N+1, \quad , \tag{A.56}$$

$$(u_0)_z - (w_0)_z = ik(1 - R)\tan(\theta)\, e^{i(kx - \omega t)} \quad . \tag{A.57}$$

Finally, within the i^{th} Biot medium, the normal solid displacement is given by

$$(u_i)_z = (\phi_{si}' + ik\psi_{si})\, e^{i(kx - \omega t)} \quad , \tag{A.58}$$

and the tangential solid displacement is

$$(u_i)_x = (ik\phi_{si} - \psi_{si}')\, e^{i(kx - \omega t)} \quad . \tag{A.59}$$

Neither of these last two quantities have counterparts within the fluid medium.

With $h_0 = 0$, all $N + 1$ interfaces are subject to the boundary conditions

$$p_i\big|_{z_i = 0} = p_{i-1}\big|_{z_{i-1} = h_{i-1}}, \quad i = 1, 2, ..., N+1 \quad , \tag{A.60}$$

$$(\sigma_i)_{xz}\big|_{z_i = 0} = (\sigma_{i-1})_{xz}\big|_{z_{i-1} = h_{i-1}}, \quad i = 1, 2, ..., N+1 \quad , \tag{A.61}$$

$$(\sigma_i)_{zz}\big|_{z_i = 0} = (\sigma_{i-1})_{zz}\big|_{z_{i-1} = h_{i-1}}, \quad i = 1, 2, ..., N+1 \quad , \tag{A.62}$$

$$\left[(u_i)_z - (w_i)_z\right]\Big|_{z_i = 0} = \left[(u_{i-1})_z - (w_{i-1})_z\right]\Big|_{z_{i-1} = h_{i-1}}, \quad i = 1, 2, ..., N+1 \quad , \tag{A.63}$$

and the Biot/Biot interfaces are subject to the additional two boundary conditions given by

$$(u_i)_z\big|_{z_i=0} = (u_{i-1})_z\big|_{z_{i-1}=h_{i-1}}, \qquad i=2,3,\ldots,N+1 \quad , \tag{A.64}$$

$$(u_i)_x\big|_{z_i=0} = (u_{i-1})_x\big|_{z_{i-1}=h_{i-1}}, \qquad i=2,3,\ldots,N+1 \quad . \tag{A.65}$$

The transmitted and reflected fast, slow, and shear wave amplitudes within each medium are determined by substituting Eqs. (A.42), (A.43), (A.44), and (A.49) into the above six boundary conditions and solving the resulting set of linear algebraic equations for *R*, and the *A*s, *B*s, and *C*s.

This page intentionally left blank.

APPENDIX B

REDUCING THE COMPUTATIONAL COMPLEXITY OF THE PROBLEM

This page intentionally left blank.

PREVIEW

In the process of this investigation, a method was discovered that dramatically simplifies the computational complexity of the problem described in Appendix A. Prior to this discovery, an *N*-layer problem required solving a (6*N*+4)x(6*N*+4) banded matrix equation. Problems with several hundred layers would require a few hours to run on a Sun 2000. With the new simplifications a 500-layer calculation can now be performed in just over 6 minutes. This leap in computational efficiency was made possible by reducing the problem to a 4x4 matrix calculation:

$$(\mathbf{M} \mid \mathbf{PS_N C})\,\mathbf{x} \;=\; \mathbf{b} \quad , \tag{B.1}$$

where the 4x4 matrix $(\mathbf{M} \mid \mathbf{PS_N C})$ consists of a 4x1 matrix **M,** which depends solely on the properties of the fluid half-space overlayer, augmented with a 4x3 matrix $\mathbf{PS_N C}$, which is the product of three matrices:

(1) a 4x6 prefix matrix **P** that is independent of fluid, sediment, or semi-infinite Biot layer properties,

(2) a 6x6 matrix $\mathbf{S_N}$ that depends solely on the *N*-layered sediment properties,

(3) a 6x3 matrix **C** that depends solely on the semi-infinite Biot layer properties.

The 4-vector **x** contains the solution for the reflection coefficient and the three transmission coefficients for the Biot fast, slow, and shear waves through the *N* sediment layers. The 4-vector **b** depends solely on the properties of the fluid overlayer.

The sediment matrix $\mathbf{S_N}$ contains all the layered sediment information, and has the following simple form:

$$\mathbf{S_N} \;=\; \mathbf{L_1 L_2 L_3 \ldots L_N} \quad , \tag{B.2}$$

where the 6x6 matrix $\mathbf{L_i}$ depends solely on the properties of the i^{th} sediment layer. And $\mathbf{L_i}$, in turn, can be written as

$$\mathbf{L_i} = \mathbf{B_i D_i^{-1} B_i^{-1}} \quad , \tag{B.3}$$

where the 6x6 matrix $\mathbf{B_i}$ depends solely on the material properties of the i^{th} Biot sediment layer and $\mathbf{D_i}$ is a diagonal 6x6 matrix depending on both the material properties and the thickness of the i^{th} layer. All the layer thickness information is contained in the $\mathbf{D_i}$'s.

METHOD

Given the definition of the reflection and transmission coefficients for the i^{th} layer, as displayed in Eqs. (A.42) - (A.44), we define the vectors $\mathbf{v_i}$ by

$$\mathbf{v_i} = \begin{pmatrix} A_{+si} \\ B_{+si} \\ C_{+si} \\ A_{-si} \\ B_{-si} \\ C_{-si} \end{pmatrix}, \quad \mathbf{i = 1, 2, 3, ..., N} \quad , \tag{B.4}$$

$$\mathbf{v_{N+1}} = \begin{pmatrix} A_{+sN+1} \\ B_{+sN+1} \\ C_{+sN+1} \end{pmatrix} \quad . \tag{B.5}$$

The values of $\mathbf{v_i}$ and $\mathbf{v_{i+1}}$ are related by the boundary conditions supplied in Eqs. (A.60) - (A.65). These equations can be recast in matrix-vector form as

$$\mathbf{A_i v_i} = \mathbf{B_{i+1} v_{i+1}}, \quad \mathbf{i = 1, 2, 3, ..., N-1} \quad , \tag{B.6}$$

$$\mathbf{A_N v_N} = \mathbf{C v_{N+1}} \quad , \tag{B.7}$$

where $\mathbf{A_i}$ and $\mathbf{B_{i+1}}$ are 6x6 matrices describing the boundary conditions at the lower surface of the $i^{\underline{th}}$ layer and the upper surface of the $(i+1)^{\underline{th}}$ layer, respectively, and **C** is a 6x3 matrix describing the boundary conditions at the surface of the Biot half-space.

Applying the coordinate system described in the paragraph following Eq. (A.18), the matrices for the $i^{\underline{th}}$ layer, $\mathbf{A_i}$ and $\mathbf{B_i}$, with layer thickness h_i, are related by

$$\mathbf{A}_i = \mathbf{B}_i \mathbf{D}_i \quad , \tag{B.8}$$

where

$$\mathbf{D}_i = \begin{pmatrix} e^{il_{1i}h_i} & 0 & 0 & 0 & 0 & 0 \\ 0 & e^{il_{2i}h_i} & 0 & 0 & 0 & 0 \\ 0 & 0 & e^{il_{si}h_i} & 0 & 0 & 0 \\ 0 & 0 & 0 & e^{-il_{1i}h_i} & 0 & 0 \\ 0 & 0 & 0 & 0 & e^{-il_{2i}h_i} & 0 \\ 0 & 0 & 0 & 0 & 0 & e^{-il_{si}h_i} \end{pmatrix} \quad , \tag{B.9}$$

and l_{1i}, l_{2i}, and l_{si} are the wave numbers of the Biot fast, slow, and shear waves, respectively. Inserting Eq. (B.8) into Eq. (B.6), and rearranging terms, yields

$$\mathbf{v}_i = \mathbf{D}_i^{-1} \mathbf{B}_i^{-1} \mathbf{B}_{i+1} \mathbf{v}_{i+1}, \qquad i = 1, 2, 3, \ldots, N-1 \quad . \tag{B.10}$$

Applying this recursively, we have

$$\mathbf{v}_1 = \mathbf{D}_1^{-1} \mathbf{B}_1^{-1} \left[\prod_{j=2}^{N-1} \left(\mathbf{B}_j \mathbf{D}_j^{-1} \mathbf{B}_j^{-1} \right) \right] \mathbf{B}_N \mathbf{v}_N \quad . \tag{B.11}$$

Inserting Eqs. (B.7) and (B.8) gives

$$\mathbf{v}_1 = \mathbf{D}_1^{-1} \mathbf{B}_1^{-1} \left[\prod_{j=2}^{N-1} \left(\mathbf{B}_j \mathbf{D}_j^{-1} \mathbf{B}_j^{-1} \right) \right] \mathbf{C} \mathbf{v}_{N+1} \quad . \tag{B.12}$$

Consider the matrix

$$\mathbf{P} = \begin{pmatrix} 1 & 0 & 0 & 0 & 0 & 0 \\ 0 & 1 & 0 & 0 & 0 & 0 \\ 0 & 0 & 1 & 0 & 0 & 0 \\ 0 & 0 & 0 & 1 & 0 & 0 \end{pmatrix} \quad . \tag{B.13}$$

Note that right-multiplying this matrix by any 6x6 matrix truncates the bottom two rows of the 6x6 matrix. Thus, if the rows of $\mathbf{B_1}$, each of which corresponds to one of Eqs. (A.60) - (A.65), are ordered in the same sequence as those equations, then the 4x6 matrix $\mathbf{PB_1}$ describes the four boundary conditions at the fluid/Biot interface of the first sediment layer. Hence, the boundary conditions at the fluid/Biot interface can be written as

$$R\mathbf{M} + \mathbf{P}\mathbf{B}_1 \mathbf{v}_1 = \mathbf{b} \quad , \tag{B.14}$$

where R is the reflection coefficient, $\mathbf{M}$ is a 4x1 matrix depending solely on the fluid properties, and $\mathbf{b}$ is a four-vector which also depends solely on the fluid properties. Inserting Eq. (B.12) into Eq. (B.13) gives

$$R\mathbf{M} + \mathbf{P}\mathbf{S}_N\mathbf{C}\,\mathbf{v}_{N+1} = \mathbf{b} \quad , \tag{B.15}$$

where

$$\mathbf{S}_N = \prod_{j=1}^{N} \left(\mathbf{B}_j \mathbf{D}_j^{-1} \mathbf{B}_j^{-1} \right) \quad . \tag{B.16}$$

Note that Eq. (B.15) can be rewritten as

$$\left(\mathbf{M} \mid \mathbf{P}\mathbf{S}_N\mathbf{C}\right) \mathbf{x} = \mathbf{b} \quad , \tag{B.17}$$

where the 4x4 matrix $(\mathbf{M} \mid \mathbf{PS_NC})$ consists of the 4x1 matrix $\mathbf{M}$ augmented with the 4x3 matrix $\mathbf{PS_NC}$, and

$$\mathbf{x} = \begin{pmatrix} R \\ A_{+sN+1} \\ B_{+sN+1} \\ C_{+sN+1} \end{pmatrix} . \qquad \text{(B.18)}$$

Thus, the problem of Appendix A can be solved quite simply and efficiently by forming the 4x4 matrix $(\mathbf{M} \mid \mathbf{PS_N C})$ and then solving for $\mathbf{x}$ in Eq. (B.19). When compared to the original $(6N+4)$x$(6N+4)$ banded matrix algorithm, with N = 500, this method consistently produced the same results to 14 out of 16 significant figures, but with a time reduction of nearly two orders of magnitude.

This page intentionally left blank.

APPENDIX C

CONVERSION FROM ONE- TO THREE-DIMENSIONAL SCATTERING STRENGTH

This page intentionally left blank.

The experimentally measured scattering at the water-sediment interface, such as the results shown by Nolle et al., is a three-dimensional process, in which energy is scattered within a hemispherical sector of 2π steradians, and the scattered intensity decreases with distance due to spreading losses. The simulations performed in this study are one-dimensional, where the scattered energy is directed back to the source of the incident wave and there is no spreading loss. In order to make quantitative comparisons between simulation and experiment, it is necessary to derive a relationship between the two processes.

The output of the one-dimensional simulation is essentially the reflected plane wave signal from the sediment interface. The coherent part is identically the reflection coefficient, and the random part may be considered as the scattered component. They are approximately equal to the reflection coefficient at normal incidence, that can be experimentally measured using a real source and receiver, after properly accounting for the spreading loss. The reflection equation is as follows: Let S_L be the source level of an acoustic source incident normally on a sediment surface. Let R_{Lc} and R_{Lr} be the coherent and random parts of the reflected signal. Let both source and receiver be at a distance r from the sediment surface. The coherent R_c and random R_r parts of the reflection coefficient amplitude, in decibels, are given by

$$R_c = R_{Lc} - S_L + 20 \log(2r) + 2\alpha r \quad , \tag{C.1}$$

$$R_r = R_{Lr} - S_L + 20 \log(2r) + 2\alpha r \quad , \tag{C.2}$$

where α is the absorption coefficient.

When computed as backscattering strength, the corresponding coherent and random components are defined as follows.

$$S_c = R_{Lc} - S_L + 40 \log(r) + 2\alpha r - 10 \log(A) \quad , \tag{C.3}$$

$$S_r = R_{Lr} - S_L + 40 \log(r) + 2\alpha r - 10 \log(A) \quad , \tag{C.4}$$

where A is the insonified area.

Subtracting Eqs.(C.1) and (C.2) from (C.3) and (C.4), the difference between the reflected levels generated by the one-dimensional simulation, and the scattered strengths measured in the laboratory, is given by

$$R_c - S_c = R_r - S_r = 20 \log(2) + 10 \log(A) - 20 \log(r) \quad . \qquad (C.5)$$

The insonified area is defined by the beamwidth of the combined projector-receiver combination. Let us define the beamwidth θ such that

$$A = (\theta r)^2 \quad . \qquad (C.6)$$

Then, the conversion from one- to three-dimensional scattering strength is expressible in terms of the beamwidth only,

$$R_c - S_c = R_r - S_r = 20 \log(2) + 10 \log(\theta^2) \quad . \qquad (C.7)$$

From the measurement of reflection loss (-11 dB) and the peak of backscattering strength plot in Fig. 23 of Nolle et al., the value of $R_c - S_c$ for their experimental apparatus, at 1 MHz, is found to be

$$R_c - S_c = -11 - 22 = -33 \text{ dB} \quad . \qquad (C.8)$$

Substituting into Eq. (C.7), the effective system half-beamwidth at 1 MHz is found to be

$$\theta = 0.011 \text{ radians} \quad . \qquad (C.9)$$

An approximate expression for the combined -3 dB beamwidth of source and receiver is given as follows.

$$\sin(\theta)\sqrt{2} = 0.443 \lambda / D \quad , \qquad (C.10)$$

where λ is the acoustic wavelength and D the diameter of the aperture, and the $\sqrt{2}$ factor accounts for the cumulative effect of the projector and receiver apertures.

As a check, substituting from Eq. (C.9) into (C.10), it is found that the aperture of both source and receiver must have been approximately 4 cm, which is consistent with the stated transducer diameter of 1.5 in. used in the experiment.

For narrow beams, the beamwidth is inversely proportional to the frequency; therefore, the conversion from one- to three-dimensional scattering strength at 500 kHz is estimated to be

$$R_C - S_C = -33 \text{ dB} + 10 \log(4) = -27 \text{ dB} \quad .$$

This page intentionally left blank.

REFERENCES

1. D. R. Jackson, S. P. Winebrenner, and A. Ishimaru, "Application of Composite Roughness Model to High-Frequency Bottom Backscattering," J. Acoust. Soc. Am. 79(5), 1410-1422 (1986).

2. A. N. Ivakin and Yu. P. Lysanov, "Underwater Sound Scattering by Volume Inhomogeneities of a Bottom Bounded by a Rough Surface," Sov. Phys. Acoust. 27(3), 212-215 (1981).

3. P. C. Hines, "Theoretical Model of Acoustic Backscatter from a Smooth Seabed," J. Acoust. Soc. Am. 88(1), 324-334 (1990).

4. N. P. Chotiros, "Biot Model of Sound Propagation in Water Saturated Sand," J. Acoust. Soc. Am. 97(1), 199-214 (1995).

5. N. P. Chotiros, "High Frequency Bottom Penetration: Panama City Experiment Analysis III," Applied Research Laboratories Technical Report No. 91-18 (ARL-TR-91-18), Applied Research Laboratories, The University of Texas at Austin, 1 July 1991.

6. N. P. Chotiros, "High Frequency Acoustic Penetration Analysis," Applied Research Laboratories Technical Report No. 89-28 (ARL-TR-89-28), Applied Research Laboratories, The University of Texas at Austin, 5 May 1989.

7. M. A. Biot, "Theory of Propagation of Elastic Waves in a Fluid-Saturated Porous Solid, I. Low-frequency Range," J. Acoust. Soc. Am. 28, 168-178 (1956).

8. M. A. Biot, "Theory of Propagation of Elastic Waves in a Fluid-Saturated Porous Solid, II. Higher Frequency Range," J. Acoust. Soc. Am. 28, 179-191 (1956).

9. M. Stern, A. Bedford, and H. R. Millwater, "Wave Reflection from a Sediment Layer with Depth Dependent Properties," J. Acoust. Soc. Am. 77(5), 1781-1788 (1985).

10. A. W. Nolle et al., "Acoustical Properties of Water-Filled Sands," J. Acoust. Soc. Am. 35(9), 1394-1408 (1963).

11. J. F. Mifsud, "Experimental Study of the Acoustic Properties of Water-Filled Sands," Defense Research Laboratory Acoustical Report No. 72 (DRL-A-72), Defense Research Laboratory (now ARL:UT), The University of Texas, October 1953.

15 September 1995

DISTRIBUTION LIST
ARL-TR-95-26
Final Report under Grant N00014-94-1-0438,
Multiple Scatter Theory of Ocean Sediments

Copy No.	
	Director Research Program Department Office of Naval Research Ballston Tower One 800 North Quincy Street Arlington, VA 22217-5660
1-3	Attn: J. Simmen (Code 321)
4	E. Chaika (Code 322)
5	W. Ching (Code 321)
6	T. Goldsberry (Code 322)
7	D. Houser (Code 333)
	Office of Naval Research San Diego Regional Office 4520 Executive Drive, Suite 300 San Diego, CA 92121-3019
8	Attn: J. Starcher, ACO
	Director Naval Research Laboratory Washington, DC 20375
9	Attn: Code 2627
10	B. Houston (Code 5136)
	DTIC-OCC Defense Technical Information Center 8725 John J. Kingman Road, Suite 0944 Fort Belvoir, VA 22060-6218
11 - 22	Attn: Library
	Commanding Officer Naval Research Laboratory Stennis Space Center, MS 39529-5004
23	Attn: E. Franchi (Code 7100)
24	S. Stanic (Code 7174)
25	D. Ramsdale (Code 7170)
26	M. Richardson (Code 7431)
27	R. Meredith (Code 7174
28	Library (Code 7032.2)

Distribution List for ARL-TR-95-26 under Grant N00014-94-1-0438 (cont'd)

Copy No.

Commander
Naval Meteorology and Oceanography Command
Stennis Space Center, MS 39529
29 Attn: D. Durham (N5A)
30 R. Martin (N5C)

Commander
Program Executive Office - Mine Warfare
Crystal Plaza Bldg 6
2531 Jefferson Davis Highway
Arlington, VA 22242-5167
31 Attn: J. Grembi (PEOMIW)
32 D. Gaarde (PMO407B)

G & C Systems Manager
MK48/ADCAP Program Office
National Center 2
2521 Jefferson Davis Hwy., 12W32
Arlington, VA 22202
33 Attn: H. Grunin (PMO402E1)

Program Manager
MK50 Torpedo Program Office
Crystal Park 1
2011 Crystal Drive, Suite 1102
Arlington, VA 22202
34 Attn: A. Knobler (PMO406B)

Commander
Dahlgren Division
Naval Surface Warfare Center
Dahlgren, VA 22448-5000
35 Attn: Library

Commander
Dahlgren Division
Naval Surface Warfare Center
Silver Spring, MD 20903-5000
36 Attn: S. Martin (G94)
37 J. Sherman (N50)
38 M. Stripling (N04W)

Distribution List for ARL-TR-95-26 under Grant N00014-94-1-0438 (cont'd)

Copy No.

Director
Applied Physics Laboratory
The University of Washington
1013 N.E. 40th Street
Seattle, WA 98105

39 Attn: R. Spindel
40 D. Jackson
41 K. Williams
42 S. Kargl

Director
Life Sciences Directorate
Office of Naval Research
Arlington, VA 22217-5000

43 Attn: S. Zornetzer (Code 114)

Director
Marine Physical Laboratory
The University of California, San Diego
San Diego, CA 92152

44 Attn: K. Watson
45 C. de Moustier

Commander
Mine Warfare Command
325 Fifth St. SE
Corpus Christi, TX 78419-5032

46 Attn: G. Pollitt (Code N02R)

Applied Research Laboratory
The Pennsylvania State University
P.O. Box 30
State College, PA 16804-0030

47 Attn: L. Hettche
48 R. Goodman
49 E. Liszka
50 D. McCammon
51 F. Symons
52 Library

Distribution List for ARL-TR-95-26 under Grant N00014-94-1-0438 (cont'd)

Copy No.

Commanding Officer
Coastal Systems Station, Dahlgren Division
Naval Surface Warfare Center
Panama City, FL 32407-5000
53 Attn: M. Hauser (Code 10CD)
54 R. Lim (Code 130B)
55 E. Linsenmeyer (Code 10P)
56 D. Todoroff (Code 130)

Commander
Naval Undersea Warfare Center Division
New London, CT 06320-5594
57 Attn: J. Chester (Code 3112)
58 P. Koenig (Code 33A)

Advanced Research Projects Agency
3701 North Fairfax Drive
Arlington, VA 22203-1714
59 Attn: W. Carey

Commander
Naval Undersea Warfare Center Division
Newport, RI 02841-5047
60 Attn: J. Kelly (Code 821)
61 F. Aidala (Code 842)
62 W. Gozdz (Code 843)

Physics Department
The University of Texas at Austin
Austin, TX 78712
63 Attn: T. Griffy

Aerospace Engineering Department
The University of Texas at Austin
Austin, TX 78712
64 Attn: M. Bedford
65 M. Stern

66 Robert A. Altenburg, ARL:UT

67 Hollis Boehme, ARL:UT

68 Frank A. Boyle, ARL:UT

Distribution List for ARL-TR-95-26 under Grant N00014-94-1-0438 (cont'd)

Copy No.	
69	Nicholas P. Chotiros, ARL:UT
70	John M. Huckabay, ARL:UT
71	Thomas G. Muir, ARL:UT
72	Dennis J. Yelton, ARL:UT
73	Library, ARL:UT
74 - 78	Reserve, ARL:UT